CHEMISTRY
A EUROPEAN JOURNAL

DOI: 10.1002/chem.201001083

# Micro- to Macroscopic Observations of MnAlPO-5 Nanocrystal Growth in Ionic-Liquid Media

**Eng-Poh Ng,[a, d] Lama Itani,[b] Satpal Singh Sekhon,[c] and Svetlana Mintova*[d]**

**Abstract:** Micro- and macroscopic studies of nucleation and growth processes of MnAlPO-5 nanosized crystals under ionothermal synthesis conditions are reported herein. The samples treated at 150 °C were extracted from the reaction mixture at various stages of crystallization, and characterized by XRD; SEM; thermogravimetric analysis (TGA); $^{31}P$ and $^{27}Al$ solid-state magic angle spinning (MAS) NMR, Raman, UV/Vis, and X-ray fluorescence spectroscopy (XRF). The starting raw materials (alumina, manganese, and phosphorous) were dissolved completely in the ionic liquid and transformed into an amorphous solid after 5 h of ionothermal treatment. This amorphous solid then undergoes structural changes over the following 5–25 h, which result in an intermediate phase that consists of octahedral Al species linked to the manganese and phosphate species. The first MnAlPO-5 nuclei on the surface of the intermediate can be observed after 50 h ionoheating. These nuclei further grow, as the surface of the intermediate is in full contact with the ionic liquid, to give crystalline MnAlPO-5 nanoparticles with a mean diameter of 80 nm. The crystals become fully detached from the intermediate and are then liberated as discrete particles after 90 h heating. The transformation process from amorphous to intermediate and then to the crystalline MnAlPO-5 nanoparticles shows that nucleation starts at the solid–liquid interface and continues through surface-to-core reversed-growth until the entire amorphous solid is transformed into discrete nanocrystals.

**Keywords:** crystal growth · ionic liquids · ionothermal synthesis · nanoparticles · zeolites

## Introduction

Zeolite and zeotype-based molecular sieves represent one of the most significant groups of inorganic materials, largely because of their importance in industrial applications such as sorption, green chemistry, ion-exchange, and, catalysis.[1] In general, these materials are prepared by hydrothermal treatment under autogenous pressure from highly alkaline reaction mixtures.[2,3] In many cases the synthesis of molecular sieves requires the presence of organic agents (quaternary ammonium salts, amines, etc.), which may play the role of pore fillers or templates to direct the crystallization towards the formation of a specific structure.[4]

Ionothermal synthesis based on ionic liquids (ILs) as both solvent and template has been recently applied in the preparation of micron-sized porous materials. This approach utilizes the unique chemical properties of the ILs, such as their extremely low vapor pressure, high ionic conductivity, and strong ability to dissolve organic and inorganic compounds.[5,6] However, the preparation of molecular sieves in ILs has so far not been exploited to its full potential, because crystallization proceeds in a different manner from the hydrothermal synthesis pathway. During the ionothermal synthesis, the reaction takes place in an ionic environment (only cations and anions); this is different from the hydrothermal technique, in which the solvent is predominantly molecular. Therefore, new insight into the crystallization of porous nanomaterials in ionothermal systems is necessary to achieve better control over the crystallization, and for the design of new crystalline phases.

[a] Dr. E.-P. Ng
School of Chemical Sciences, Universiti Sains Malaysia
11800 USM, Pulau Pinang (Malaysia)

[b] L. Itani
Institut de Science des Matériaux de Mulhouse (IS2M)
LRC CNRS 7228, Université de Haute Alsace, ENSCMu
3 rue Alfred Werner, 68093 Mulhouse (France)

[c] Prof. S. S. Sekhon
Department of Physics, Guru Nanak Dev University
Amritsar 143005, Punjab (India)

[d] Dr. E.-P. Ng, Dr. S. Mintova
Laboratoire Catalyse & Spectrochimie, ENSICAEN
Université de Caen, CNRS, 6 boulevard du Maréchal Juin
14050 Caen (France)
E-mail: svetlana.mintova@hotmail.com

Pure aluminophosphate (AlPO-*n*) with AEL-, AFI-, ATV-, and SOD-type structures have previously been synthesized by using various types of ILs.[7,8] Tetravalent and/or transition metals (Si, Co, Fe, etc.) have been incorporated in the AlPO-*n* framework, which has led to redox and catalytic activities.[9–11] Moreover, ILs are excellent solvents for the initial inorganic species, thus enabling them to be used as an alternative to the tetraalkylammonium cations in the preparation of microporous materials.

Herein, nanosized, manganese-containing aluminophosphate number 5 (MnAlPO-5 with AFI topology) was synthesized in the presence of 1-ethyl-2,3-dimethylimidazolium bromide ([edmim]Br) IL[12] under ambient conditions. The entire process, from the formation of amorphous solids through transformation into intermediates and crystallization of the discrete nanosized MnAlPO-5 material, was observed on micro- and macroscopic levels.

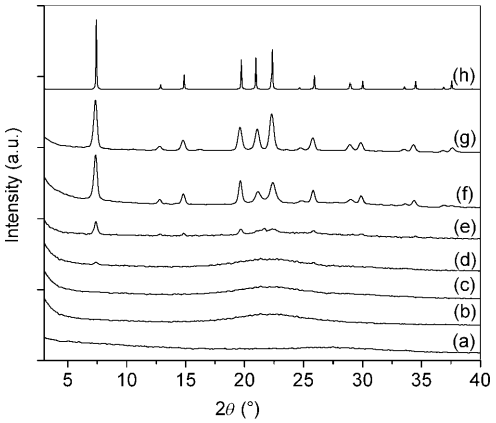


Figure 1. Powder XRD patterns of samples after ionothermal treatment at 150 °C for a) 5 min, b) 5 h, c) 25 h, d) 50 h, e) 70 h, f) 80 h, and g) 90 h. h) reference AlPO-5.

## Results and Discussion

**Observation of macroscopic growth of MnAlPO-5 nanocrystals in IL media**: The growth of MnAlPO-5 nanocrystals in an ionic environment at 150 °C was interrupted at various intervals, and the solids were extracted and subjected to characterization. Partial dissolution of the starting chemical reagents in the IL was observed during the first 5 min of heating; complete dissolution was achieved after 5 h. About 94.7 and 15.5 wt % of solids were separated from the reaction suspensions after 5 min and 5 h, respectively (Table 1).

Table 1. Synthesis conditions for MnAlPO-5 nanocrystals.

| Phase | Heating time [h] | Mass of solid [mg] | Mass of solid [wt %] | Mn/P ratio ($10^{-2}$) | Crystallinity [%][a] |
|---|---|---|---|---|---|
| amorphous | 0.083 | 147.5 | 94.7 | 76.8 | – |
| intermediate | 5 | 24.1 | 15.5 | 1.4 | 0 |
| | 25 | 30.9 | 19.8 | 3.1 | 0 |
| intermediate & crystalline solids | 50 | 34.3 | 22.0 | 3.8 | 6 |
| | 70 | 45.5 | 29.2 | 4.2 | 23 |
| crystalline solids | 80 | 62.1 | 39.9 | 5.3 | 90 |
| | 90 | 61.3 | 39.3 | 5.3 | 100 |

[a] Reference sample: crystalline MnAlPO-5 after 90 h heating at 150 °C.

On increasing the reaction time from 5 to 25 h, the amount of solids extracted from the reaction mixture increases to 19.8 wt %; however, the samples were amorphous according to the XRD data (Figure 1a, b, and c). A broad amorphous band in the region of $2\theta = 17$–$27°$ in the X-ray patterns implies that no crystalline structure is formed in the reaction mixture during the first 25 h of heating. Further heating from 50 to 70 h results in an increase in the amount of solids recovered from 22 to 29.2 wt %; a constant mass of solid sample (about 39 wt %) is recovered after 80 h of heating (see Table 1). The first Bragg peak at $2\theta = 7.47°$ appears in spectrum after 50 h of heating (Figure 1d). All other Bragg peaks characteristic of the AFI-type structure appear over the following 20 h, and their intensity increases gradually up to 90 h.[14] The diffraction patterns of the MnAlPO-5 samples contain broader reflections than those of the micron-sized AFI material (Figure 1h), which indicates the formation of small crystals. The degree of crystallinity of the samples is calculated from the change in intensity of the three peaks at $2\theta = 7.47$, 19.85, and 22.46° relative to the reference sample, and the results are summarized in Table 1. About 90 % crystallinity has been achieved for the sample heated for 80 h, while a completely crystalline (100 %) sample is obtained after 90 h of ionothermal treatment (Figure 1g).

The change in morphology of the samples on heating was followed by SEM. For each sample two micrographs at different magnifications are depicted in Figure 2. After 5 min of heating, an amorphous solid can be seen. The morphology of the solid starts to change after 5 h of heating, when intermediates with more pronounced structural features can be seen on the top of the isolated solids (Figure 2e, f). The morphology of the intermediates changes visibly after 50 h of heating (Figure 2g, h). At this stage, the sample contains crystalline phase, which can also be detected by XRD (see Figure 1d). After 70 h, the formation of long waferlike particles containing both the intermediate and the crystalline solids can seen (Figure 2i, j). Finally, the amorphous solids are transformed into discrete MnAlPO-5 nanocrystals after 80 h treatment (see Figure 2k, l). The average size of the nanocrystals in this sample is about 60–80 nm, and the particles are strongly attached to the intermediate. A progressive liberation of discrete crystalline nanoparticles with a monomodal particle size distribution is observed after 90 h of heating (Figure 2m, n). The nanosized MnAlPO-5 crystals prepared by ionothermal pathway for 90 h are spheroidal rather than needle-shaped, which is the more common mor-

  

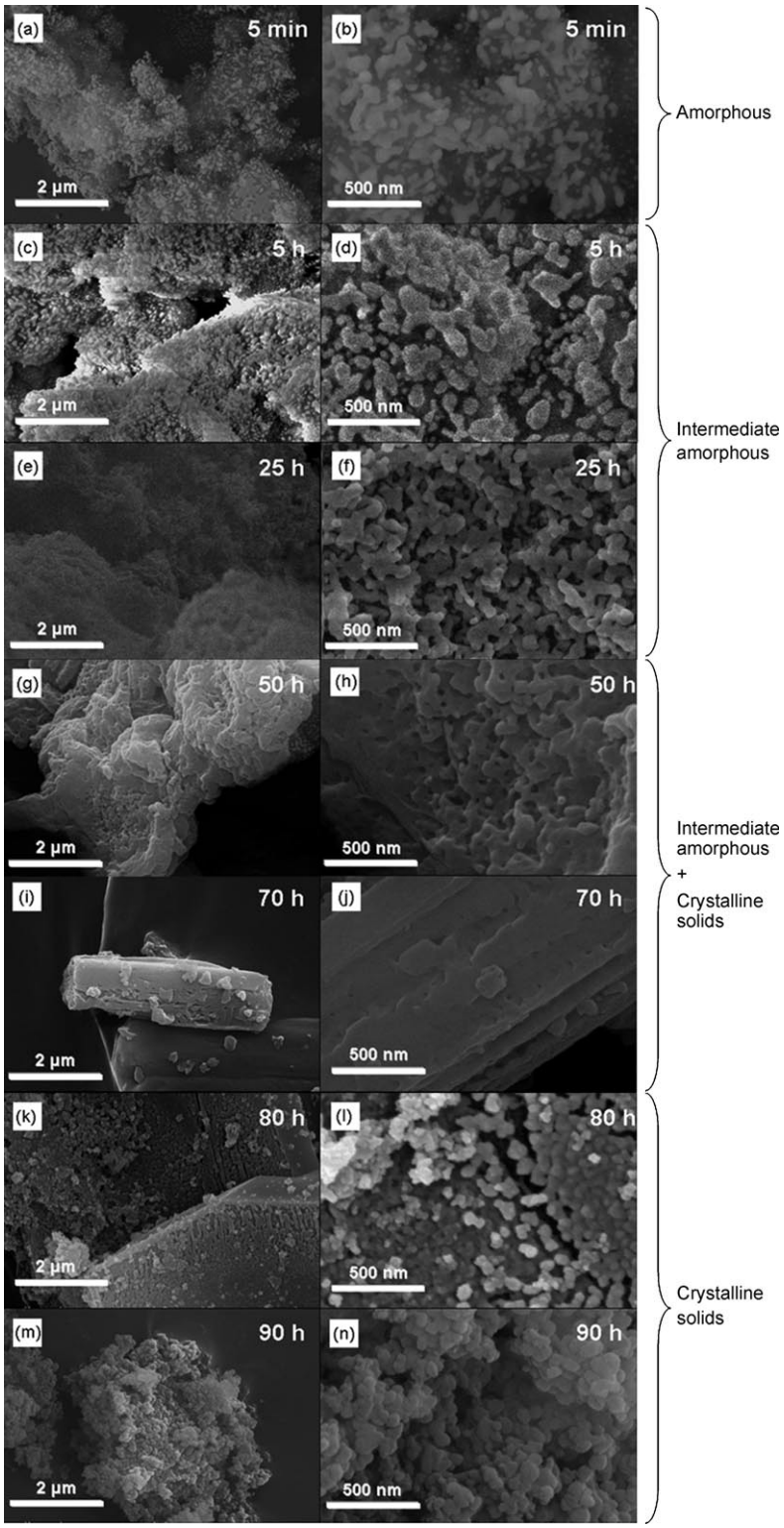


Figure 2. SEM images of samples recovered after heating at 150 °C for a),b) 5 min, c),d) 5 h, e),f) 25 h, g),h) 50 h, i),j) 70 h, k),l) 80 h, and m),n) 90 h. Scale bar left: 2 μm, right: 500 nm.

phology for AlPO-5 crystals synthesized under conventional hydrothermal heating.[15] Separate, fully crystalline particles make up about 39 wt% of the reaction mixture at 80 and 90 h.

**Microscopic observation of growth of MnAlPO-5 nanocrystals in IL media**: The microscopic properties of the framework are directly related to the macroscopic properties of the crystalline material. Therefore, an intensive investigation into the changes in the ionic liquid, Al, P, and Mn components during the crystallization of MnAlPO-5 nanocrystals was carried out. $^{31}P$ and $^{27}Al$ MAS NMR spectra characterize the local environments of P and Al in the solids at various stages of heating (see Figure 3). A non-symmetric broad signal at $\delta =$ 5.5 ppm is observed in the sample after 5 min heating, which is attributed to the low-symmetry six-coordination of aluminum in prehydrolyzed Al species (Al–O*i*Pr) (Figure 3a). The hydrolyzation of Al alkoxide species in the IL is almost complete after 5 h, and the signal at $\delta = 5.5$ ppm has almost disappeared (see Figure 3b). This indicates that the Al species from the alkoxides has been completely liberated (dissolved) in the IL. Two new signals at $\delta = 40.6$ and $-11.6$ ppm appear in the spectrum of the sample treated for 5 h. The first signal is assigned to tetrahedral aluminum in an amorphous MnAlPO matrix, while the second signal is in the region where the octahedral aluminum due to $Al(PO)_4(OH_2)_2$ species appears (Figure 3b).[16] After the ionothermal heating for 25 h, the signal at $\delta = 40.6$ ppm has disappeared and the octahedral Al signal has shifted upfield to $\delta = -13.2$ ppm, which corresponds to A1 coordinated with six $PO_4$ tetrahedra in Al-$(H_2PO_4)$ (Figure 3c).[16] This indicates that the coordination environment of Al has changed on heating, and an increasing number of $PO_4$ tetrahedra are linked to octahedral Al atoms in favor of OH groups or water molecules.[17] As a result, a new intermediate (still amorphous) phase with different morphology is formed. The

  

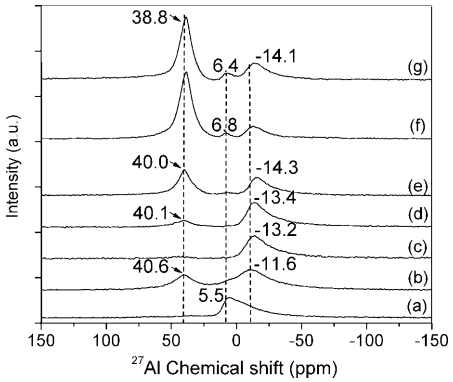


Figure 3. $^{27}$Al MAS NMR spectra of solid samples heated at 150°C for a) 5 min, b) 5 h, c) 25 h, d) 50 h, e) 70 h, f) 80 h, and g) 90 h.

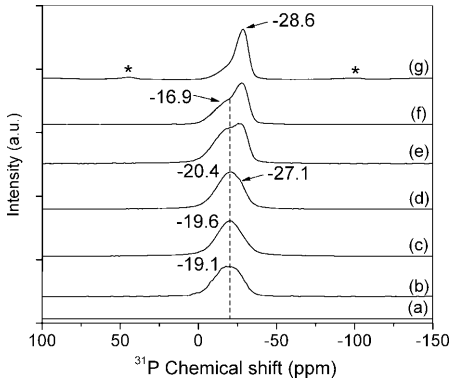


Figure 4. $^{31}$P MAS NMR spectra of samples heated at 150°C for a) 5 min, b) 5 h, c) 25 h, d) 50 h, e) 70 h, f) 80 h, and g) 90 h. * indicates spinning sidebands.

changes in the $^{27}$Al MAS NMR spectra are in a good agreement with the changes observed by the SEM and XRD analyses on the macroscopic level (Figures 1 and 2). On increasing the duration of ionothermal treatment to 50 h, a new weak signal in the region for tetrahedral aluminum appears at $\delta = 40.1$ ppm (Figure 3d). The $^{27}$Al MAS NMR spectra of the samples after 70, 80, and 90 h of ionothermal treatment contain a signal at about $\delta = 40.0$ ppm that increases gradually and becomes dominant after 80 h (Figure 3e). The signal also shifts gradually to $\delta = 38.8$ ppm, which suggests that the tetrahedral Al is in a different chemical environment in the fully crystalline MnAlPO-5.[19]

On the other hand, the octahedral Al signal shifts upfield from $\delta = -13.4$ to $-14.3$ ppm after 70 h heating (Figure 3e). This shift is due to the different chemical environments around the octahedral Al atoms in the amorphous and crystalline parts of the solid samples, as observed by XRD and SEM on the macroscopic level. Meanwhile, a new signal at $\delta = 6.8$ ppm was detected after 70 h, which was assigned to pentacoordinated aluminum, formed upon water adsorption.[20] Furthermore, the line widths of the tetrahedral ($\delta =$ 38.8 ppm), pentahedral ($\delta = 6.4$ ppm), and octahedral ($\delta =$ $-14.3$ ppm) aluminum signals decrease with increasing heating time, which indicates greater ordering and a higher degree of crystallinity in the material (Figure 3g).

The development of the $^{31}$P MAS NMR spectra of the samples over the heating period is shown in Figure 4. No signal is observed in the sample heated for 5 min, which indicates that the P is still present in the liquid phase, and that no amorphous aluminophosphate has yet been formed (Figure 4a). A broad signal is detected at $\delta = -19.1$ ppm after 5 h, which shows that an amorphous manganoaluminophosphate composed of tetrahedrally coordinated P sites of $P(OH)_2(OAl_{tet})_2$ and $P(OH)_2(OAl_{tet})(OAl_{oct})$ is formed (Figure 4b).[18] Upon ionothermal treatment for 25 h, these local environments have fully evolved to become $P(OH)(OAl_{oct})_3$, which results in an upfield shift to $\delta = -19.6$ ppm (Figure 4c). The signal remains broad, which suggests the material is amorphous. After heating for 50 h, a signal at $\delta =$ $-20.4$ ppm, along with a shoulder at $\delta = -27.1$ ppm, begins to emerge in the spectrum (Figure 4d). These signals are ascribed to P sites connected with both tetrahedral and octahedral Al sites, which are present in both the amorphous or crystalline solids.[18] This sample contains intermediates and crystalline solids as stated from the SEM and XRD observations (see Figures 1 and 2).

The $^{31}$P MAS NMR spectra of the samples after 70, 80, and 90 h are shown in Figure 4e–g). Two bands at $\delta = -16.9$ and $-27.1$ ppm can be seen for the signal assigned to tetrahedral P sites after 70 h. After 80 h the signal has split; the intensity of the first signal has decreased, but the latter signal has increased. This indicates that the amorphous or disordered material has been transformed into crystalline MnAlPO-5. This result is consistent with the increase in intensity of the Bragg diffraction peaks in the XRD patterns (Figure 1), and with the appearance of the signal corresponding to the tetrahedral Al sites in the $^{27}$Al MAS NMR spectra (Figure 3). The signal at $\delta = -16.9$ ppm decreases with increasing crystallization time, and after 90 h a strong line at $\delta = -28.6$ ppm characteristic of the unique tetrahedral environment of phosphorus can be observed.[21]

The various amorphous, intermediate, and crystalline samples were also studied by diffuse reflectance UV/Vis spectroscopy. The spectra are depicted in Figure 5. The spectrum for pure AlPO-5 reference sample (Figure 5h) is also provided for comparison. After heating for 5 min the spectrum exhibits three bands at 220, 264, and 308 nm. The peak at 220 nm can be assigned to Al–O charge transfer.[22,23] The intensity and position of this peak varies, depending on several factors such as aluminum and oxygen charge density, Al–O distance, the crystallographic positions of the aluminum atoms in the framework, and the surroundings ($H_2O$ and organics give rise to different wavelengths and intensities for the charge-transfer peak).[24] The second signal at 264 nm is characteristic of bulk manganese oxide, while the third signal at 308 nm is assigned to an $O^{2-} \rightarrow Mn^{3+}$ charge transfer at an octahedrally coordinated site (Figure 5a).[25] The peak at 264 nm disappears from the spectrum after 5 h, whereas the peak at 308 nm shifts to 312 nm with increasing heating time. After 25 h, two new signals at 240 and 288 nm appear in the spectrum. These bands can be assigned to

  

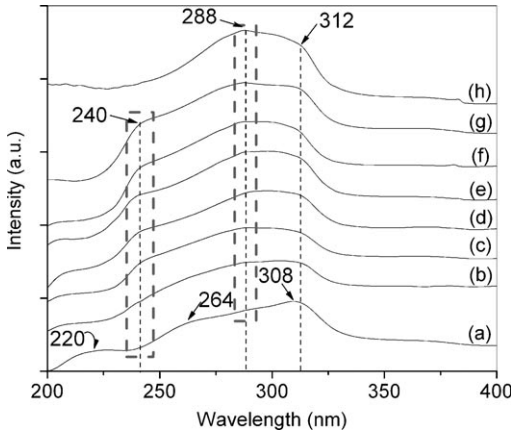


Figure 5. UV/Vis spectra of samples heated at 150 °C for a) 5 min, b) 5 h, c) 25 h, d) 50 h, e) 70 h, f) 80 h, and g) 90 h. h) reference AlPO-5.

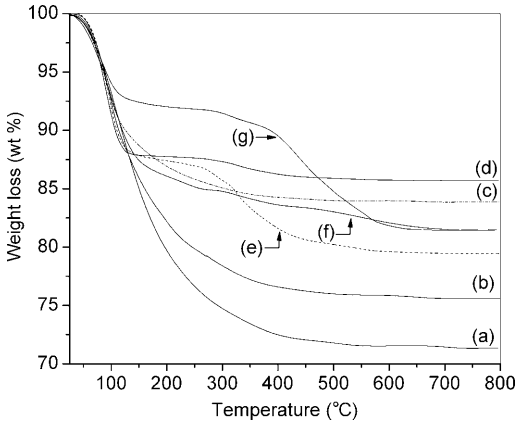


Figure 7. TGA curves of samples heated at 150 °C for a) 5 min, b) 5 h, c) 25 h, d) 50 h, e) 70 h, f) 80, and g) 90 h.

$O^{2-} \rightarrow Mn^{2+}$ and $O^{2-} \rightarrow Mn^{3+}$ charge transfers for manganese atoms in tetrahedral oxygen coordination environments; thus, the bands confirm the presence of Mn in the intermediate.[25–28] More importantly, the intensity of these signals rises gradually with an increasing Mn/P ratio in the solids during heating (Table 1), and becomes constant after 80 h of heating (Figure 5f and Table 1). No signal was observed at 500 nm (not shown), which is consistent with the absence of either MnO or $Mn_3O_4$ as separate phases in the samples.[25,29]

ILs are known as effective solvents for both organic and inorganic species due to their high hydrophilicity and ionic characteristics, which are generally not available with conventional solvents.[6] [edmim]Br provides an ionic instead of molecular environment for the crystallization of MnAlPO-5.[30] The effect of [edmim]Br was studied by thermogravimetric analysis (TGA) and Raman spectroscopy (Figures 6 and 7). As was observed previously, the aluminum isopropoxide is mixed with the Mn and P sources ($Mn(OAc)_2$ and $H_3PO_4$), and they are jointly hydrolyzed and co-condensed.

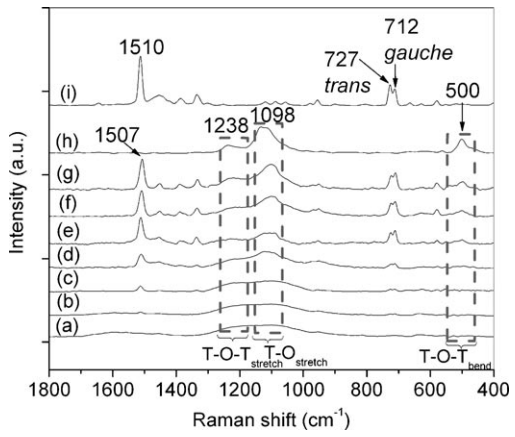


Figure 6. Raman spectra of samples heated at 150 °C for a) 5 min, b) 5 h, c) 25 h, d) 50 h, e) 70 h, f) 80 h, and g) 90 h. The spectra of reference AlPO-5 (h) and pure [edmim]Br ionic salt (i) are also provided.

The co-condensation reaction between the hydrolyzed intermediates leads to the formation of a tetrahedral active species (as revealed by $^{31}P$ and $^{27}Al$ MAS NMR spectroscopy), and then to the formation of manganoaluminophosphate (MnAlPO) oligomers. The Raman spectrum of the sample treated for only 5 h contains very weak signals at 1510, 727, and 712 $cm^{-1}$ due to C–H vibrations from the $[edmim]^+$ cations, which indicates negligible chemical interaction with the MnAlPO amorphous material. This observation is supported by TGA, in which a single-step weight loss is measured (Figure 7b).

The $[edmim]^+$ content of the solid samples increases with heating time, according to the Raman spectra (Figure 6). The characteristic bands of the AFI framework at 500, 1098, and 1238 $cm^{-1}$ are not detected in the sample even after 25 h treatment, which indicates that no crystalline MnAlPO-5 phase is formed at that stage (see Figure 6c).[13] After 50 h, the above three bands appear in the spectrum (Figure 6d), thus indicating the formation of secondary building units (SBU) characteristic of the AFI structure. The AFI structure contains alternating Al and P atoms, which form four- and six-membered rings. The resulting framework structure is composed of nonconnected parallel channels of 12-membered rings. A change from a single- to a three-step weight-loss curve is observed for the sample by TGA (see Figure 7d). The multistep weight-loss process reveals that the $[edmim]^+$ is either in the pores of the AFI crystals (410–600 °C) or is weakly bound to the intermediates (200–410 °C).[13] The weight loss for both regions becomes more pronounced for the samples with a high degree of crystallinity. After 70 h, the presence of crystalline AFI phase is indicated by both Raman and TGA data. The three characteristic bands for the AFI structure (500, 1098, and 1238 $cm^{-1}$) together with the bands assigned to the C–H vibrations of encapsulated $[edmim]^+$ cations are clearly present in the spectrum of the sample heated for 70 h. The intensity of these signals is constant after 90 h heating. Several vibration bands assigned to C–H bending modes at 1468, 1440, and 1420 $cm^{-1}$ in the pure IL are not observed in the crystalline

  

MnAlPO-5. This infers that the $[edmim]^+$ is tightly held in the pores of the AFI nanocrystals, so that its C–H bond movements are constrained.[21]

The Raman bands of the MnAlPO-5 sample are broad and redshifted, as observed in our previous work.[13] For instance, the band at 1513 $cm^{-1}$, which corresponds to the C–H bending mode of pure [edmim]Br, shifts to 1510 $cm^{-1}$ (50 h) and then to 1507 $cm^{-1}$ (90 h), along with a broadening due to the presence of nanocrystals. Similar results have been reported and attributed to phonon confinement effects and an increasing interaction of the IL molecules with the Al–O–P units.[31,32] Further, a progressive change in the relative intensities of the two bands at 727 and 712 $cm^{-1}$ for [edmim]Br in the MnAlPO-5 matrix is observed. These two bands are assigned to the $CH_3$ rocking mode from the alkyl groups, and can be used to determine the rotational isomerism of the *trans* (727 $cm^{-1}$) or *gauche* (712 $cm^{-1}$) conformers.[33–36] The *trans*/*gauche* ratio is 60:40 for the pure [edmim]Br IL, which shows that more stable *trans* conformer is spontaneously favored in nature (Figure 6i). However, the nonstable *gauche* configuration becomes dominant when the [edmim]Br IL acts as a template for the crystallization of MnAlPO-5. The *trans*/*gauche* ratio was 50:50 for the sample heated for 25 h, but the ratio changed to 45:55 for purely crystalline MnAlPO-5 after heating for 90 h. The change to the nonfavored *gauche* configuration can be explained by the occlusion of the $[edmim]^+$ in the AFI pores, because this results in close packing and, consequently, steric and torsional strains of the $[edmim]^+$ are observed.

As discussed above, the weight loss from 200–410 °C corresponds to the $[edmim]^+$ cations weakly bound to the amorphous or partially crystalline MnAlPO-5 particles. On increasing the heating time from 50 to 80 h, an increment of the weight loss from 1.4 to 5.9 wt % for that region is observed. It reaches 3.3 wt % after 90 h (Table 2). A significant increase in the weight loss from 0.4 to 7.5 wt % over the temperature interval of 410–600 °C has been measured for the same sample. This reveals that an increasing amount of $[edmim]^+$ is located in the pores of the MnAlPO-5 crystals. Therefore, the IL molecules require higher temperatures to be released from the MnAlPO-5 pores.[19] The thermal analysis shows an increase in the weight loss for the fully crystalline MnAlPO-5 sample after 90 h heating over the temperature interval of 410–600 °C, which is in full agreement with the NMR and XRD results.

Table 2. TGA data of MnAlPO-5 samples synthesized under ionothermal conditions.

| Phase | Heating time [h] | Step of weight loss [%] | Weight loss [wt %] < 200 °C | 200–410 °C | 410–600 °C | Total weight loss [wt %] |
|---|---|---|---|---|---|---|
| amorphous | 0.083 | 1 | | 28.5 | | 28.5 |
| intermediate | 5 | 1 | | 24.1 | | 24.1 |
| | 25 | 1 | | 16.0 | | 16.0 |
| intermediate & crystalline solids | 50 | 3 | 12.2 | 1.4 | 0.4 | 14.0 |
| | 70 | 3 | 14.1 | 2.4 | 1.4 | 17.9 |
| crystalline solids | 80 | 3 | 12.6 | 5.9 | 2.1 | 20.6 |
| | 90 | 3 | 8.0 | 3.3 | 7.5 | 18.8 |

**Growth mechanism for MnAlPO-5 nanocrystals in ILs**: The formation of nanocrystalline MnAlPO-5 during ionothermal synthesis is shown in Scheme 1. During the initial 5 min of heating, the raw Al, P, and Mn materials are mixed with the IL, followed by successive dissolution, which takes place between 5 min and 5 h of heating. The species formed during this stage hydrolyze and condense, thus forming the intermediates containing mono- or oligomeric species. The intermediates are composed of P–O–Al, P–O–Mn, and Mn–O–Al units; free phosphate and manganese species are also present. The intermediates undergo reorganization during ionoheating from 5 to 25 h, during which time most of the tetrahedral Al is converted to octahedral Al, which prefers to interact with the manganese and phosphate tetrahedra rather than with OH groups or water molecules.[17] No reactive tetrahedral Al species are formed at this stage of ionothermal treatment, and no evidence for a strong interaction between $[edmim]^+$ and the intermediate is observed. The crystallization of MnAlPO-5 nanocrystals requires further

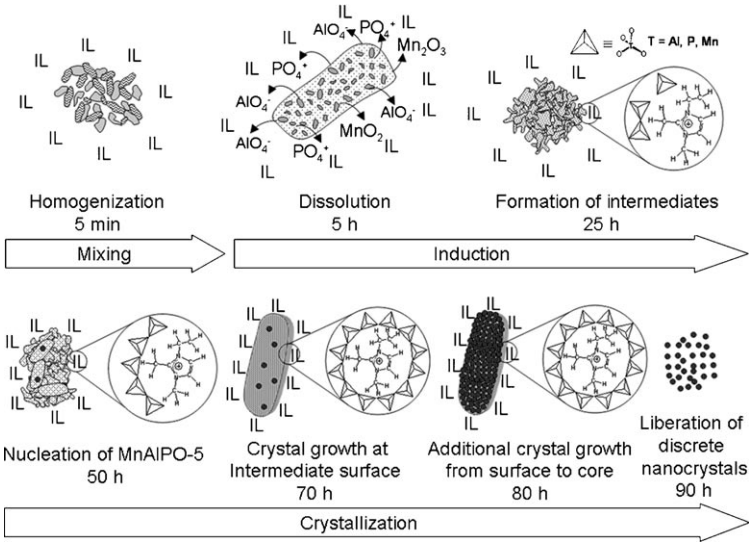


Scheme 1. The crystallization pathway of MnAlPO-5 nanocrystals under ionothermal conditions.

  

heating to promote nucleation and crystal growth. During nucleation, an extensive exchange of species between the solid and liquid components of the system takes place.

The appearance of the first AFI crystalline phase is observed after 50 h heating. At this stage, the $[edmim]^+$ cations are surrounded by the anionic species, and form a bulk solid containing partially crystalline AFI. The morphology changes after heating for 70 h. According to the macroscopic observations, the amorphous aggregates are transformed into crystalline particles after 70 h. At the microscopic level, the anionic tetrahedral MnAlPO active species enclose the $[edmim]^+$ cations through van der Waals interactions to form the initial SBU and cavities, which confine the $[edmim]^+$. An abrupt transformation of bulk amorphous into MnAlPO-5 nanocrystals takes place after 80 h. The nanocrystals (mean size of 60–80 nm) grow from the surface and remain attached to the amorphous matter and are not liberated as discrete nanoparticles at this stage. This observation reveals that nucleation takes place at the solid–liquid interface, which is also observed for zeolites with LTA- and FAU-type structures synthesized under hydrothermal treatment.[37,38,39] After 90 h of heating, crystallization through a surface-to-core reversed-growth mechanism becomes increasingly apparent once the exchange of species between the solid and liquid components of the system reaches equilibrium.[40] Discrete nanosized MnAlPO-5 crystals are formed through consumption of the large, amorphous entities as nutrients, whereas the solid mass is constant during the whole crystallization process. Finally the MnAlPO-5 nanoparticles are liberated as single crystals once the amorphous solid has been completely consumed. The resulting crystalline particles have a mean size of 80 nm and do not grow significantly after 90 h of heating.

## Conclusion

Micro- to macroscopic aspects of the crystallization process of nanosized MnAlPO-5 under ionothermal conditions have been observed. The results demonstrate that, on initial homogenization and dissolution of Al, P, and Mn sources in [edmim]Br IL, an amorphous manganoaluminophosphate (MnAlPO) is formed after 5 h of heating. Further heating (25 h) results in the hydrolyzation and condensation of the inorganic species, which leads to the formation of oligomers with an increased number of manganate and phosphate tetrahedra linked to octahedral aluminum species. During this phase, the 12-membered rings of the AFI structure start to form in the manganoaluminophosphate matrix, and confinement of the IL cations $[edmim]^+$ by the anionic MnAlPO species takes place preferably on the surface of the amorphous intermediate. The MnAlPO-5 nanocrystals grow by consuming soluble species. The resulting nanoparticles are not liberated from the amorphous surface during the first 70 h heating. Up to 90 h heating, large amorphous entities are consumed as nutrients. Fully crystalline, discrete nanosized MnAlPO-5 particles grow through a surface-to-core reversed-growth mechanism, and the single nanocrystals are finally liberated.

## Experimental Section

**Crystal growth of MnAlPO-5 nanocrystals in IL media**: A series of samples were prepared under dry, ambient conditions with a molar composition of 1:3.84:0.59:8.56:98.6 $Al_2O_3/P_2O_5/MnO_2/H_2O$/[edmim]Br.[13] Aluminum isopropoxide (0.084 g, Aldrich) and manganese(II) acetate dihydrate (0.025 g, Strem Chemicals) were placed in a round-bottomed flask (50 mL) and then mixed with [edmim]Br (4.062 g) for 1 min. Phosphoric acid (0.178 g, Riedel-de Häen) was added with stirring (250 rpm). The ionothermal treatment of the final reaction mixture was carried out at 150 °C. The solids were isolated by filtration and subjected to characterization after treatment for 5 min, 5 h, 25 h, 50 h, 70 h, 80 h, and 90 h.

**Characterization**

*Macroscopic characterization of MnAlPO-5 nanocrystals in IL media*: The crystallinity of the samples was determined by recording the XRD patterns with a Philips PW1140/90 diffractometer (step size 0.02°, $Cu_{K\alpha}$ radiation). The degree of crystallinity was calculated based on the ratio of the areas of the three most intense Bragg diffraction peaks at $2\theta$ of 7.47, 19.85, and 22.46° for each sample, in comparison to a reference sample (MnAlPO-5 heated at 150 °C for 90 h). Additionally, the crystallization process of MnAlPO-5 was also followed by TGA or differential thermal analysis recorded with a SETARAM setsys 16MS analyzer under ambient conditions with a heating rate of 5 °C $min^{-1}$ from 25 to 800 °C.

The crystal size and morphology of the samples were determined by using a Philips XL-30 SEM, while the chemical composition was analyzed with a MagiX PHILIPS PW2540 X-ray fluorescence spectrometer.

*Microscopic characterization of MnAlPO-5 nanocrystals in IL media*: The UV/Vis and Raman spectra of amorphous, intermediate, and crystalline samples were recorded with a Perkin–Elmer Lambda-35 UV/Vis spectrometer and a Bruker Equinox 55 (2000 scans, resolution of 4 $cm^{-1}$), respectively.

The $^{31}P$ and $^{27}Al$ MAS NMR spectra of the samples were recorded on a Bruker Ultrashield 400 spectrometer at MAS frequencies between 5 and 15 kHz. The $^{27}Al$ and $^{31}P$ MAS NMR spectra were obtained with 8000 scans by single pulse excitation with $\pi/12$ (0.6 μs) and $\pi/2$ (3 μs) pulses, respectively.

## Acknowledgements

Financial support from the SRIF-PNANO-ANR project is gratefully acknowledged.

[1] T. Bein, S. Mintova in *Zeolites and Ordered Mesoporous Materials, Progress and Prospects* (Ed.: J. Cejka, H. Van Bekkum), Elsevier, Amsterdam, **2005**.
[2] P. Caullet, J. L. Paillaud, A. S. Masseron, M. Soulard, J. Patarin, *Compt. Rend. Chim.* **2005**, *8*, 245.
[3] R. M. Barrer, *Hydrothermal Chemistry of Zeolites*, Academic Press, London, **1982**.
[4] H. Van Bekkum, E. M. Flanigen, J. C. Jansen, *Introduction to Zeolite Science and Practice*, Elsevier, Amsterdam, **1991**.
[5] E. R. Cooper, C. D. Andrews, P. S. Wheatley, P. B. Webb, P. Wormald, R. E. Morris, *Nature* **2004**, *430*, 1012.
[6] T. Welton, *Chem. Rev.* **1999**, *99*, 2071.
[7] L. Wang, Y. Xu, Y. Wei, J. Duan, A. Chen, B. Wang, H. Ma, Z. Tian, L. Lin, *J. Am. Chem. Soc.* **2006**, *128*, 7432.
[8] L. Han, Y. Wang, C. Li, S. Zhang, X. Lu, M. Cao, *AIChE J.* **2008**, *54*, 280.
[9] E. R. Parnham, R. E. Morris, *J. Am. Chem. Soc.* **2006**, *128*, 2204.

  

[10] Y. P. Xu, Z. J. Tian, Z. S. Xu, B. C. Wang, P. Li, S. J. Wang, Y. Hu, Y. C. Ma, K. L. Li, Y. J. Liu, J. Y. Yu, L. W. Lin, *J. Catal.* **2005**, *229–236*, 446.
[11] L. Wang, Y. P. Xu, B. C. Wang, S. J. Wang, J. Y. Yu, Z. J. Tian, L. W. Lin, *Chem. Eur. J.* **2008**, *14*, 10551.
[12] B. S. Lalia, S. S. Sekhon, *Chem. Phys. Lett.* **2006**, *425*, 294.
[13] E. P. Ng, S. S. Sekhon, S. Mintova, *Chem. Commun.* **2009**, 1661.
[14] Atlas of zeolite framework types: http://www.iza-structure.org.
[15] R. Zhao, M. Dong, Z. Qin, J. Wang, *Mater. Lett.* **2008**, *62*, 4573.
[16] C. S. Blackwell, R. L. Patton, *J. Phys. Chem.* **1988**, *92*, 3965.
[17] Y. Z. Khimyak, J. Klinowski, *Phys. Chem. Chem. Phys.* **2000**, *2*, 5275.
[18] J. G. Longstaffe, B. Chen, Y. Huang, *Microporous Mesoporous Mater.* **2007**, *98*, 21.
[19] R. A. Rakoczy, S. Ernst, M. Hartmann, Y. Traa, J. Weitkamp, *Catal. Today* **1999**, *49*, 261.
[20] R. H. Meinhold, N. J. Tapp, *Zeolites* **1991**, *11*, 401.
[21] S. P. Elangovan, V. Krishnasamy, V. Murugesan, *Catal. Lett.* **1996**, *36*, 271.
[22] E. D. Garbowski, C. Mirodatos, *J. Phys. Chem.* **1982**, *86*, 97.
[23] N. Mataga, T. Kubota, *Molecular Interactions and Electronic Spectra*, Marcel Dekker, New York, **1970**.
[24] M. A. Zanjanchi, M. K. Rashidi, *Spectrochim. Acta Part A* **1999**, *55*, 947.
[25] S. Velu, N. Shah, T. M. Jyothi, S. Sivasanker, *Microporous Mesoporous Mater.* **1999**, *33*, 61.
[26] A. Ramanathan, T. Archipov, R. Maheswari, U. Hanefeld, E. Roduner, R. Gläser, *J. Phys. Chem. C* **2008**, *112*, 7468.
[27] M. Selvaraj, P. K. Sinha, K. Lee, I. Ahn, A. Pandurangan, T. G. Lee, *Microporous Mesoporous Mater.* **2005**, *78*, 139.
[28] S. Vetrivel, A. Pandurangan, *J. Mol. Catal. A* **2006**, *246*, 223.
[29] Y. Wang, Q. Zhang in *Leading Edge Catalysis Research* (Ed.: L. P. Bevy), Nova Science Publishers, New York, **2005**.
[30] E. A. Parnham, R. E. Morris, *Acc. Chem. Res.* **2007**, *40*, 1005.
[31] J. Zuo, C. Xu, Y. Liu, Y. Qian, *Nanostruct. Mater.* **1998**, *10*, 1331.
[32] M. Ludvigsson, J. Lindgren, J. Tegenfeldt, *J. Mater. Chem.* **2001**, *11*, 1269.
[33] C. Naudin, F. Bonhomme, J. L. Bruneel, L. Ducasse, J. Grondin, J. C. Lassègues, L. Servant, *J. Raman Spectrosc.* **2000**, *31*, 979.
[34] M. G. O'Brien, A. M. Beale, C. R. A. Catlow, B. M. Weckhuysen, *J. Am. Chem. Soc.* **2006**, *128*, 11744.
[35] H. Katayanagi, S. Hayashi, H. Hamaguchi, K. Nishikawa, *Chem. Phys. Lett.* **2004**, *392*, 460.
[36] R. Ozawa, S. Hayashi, S. Saha, A. Kobayashi, H. Hamaguchi, *Chem. Lett.* **2003**, *32*, 948.
[37] B. Xie, J. Song, L. Ren, Y. Ji, J. Li, F. S. Xiao, *Chem. Mater.* **2008**, *20*, 4533.
[38] S. Mintova, N. H. Olson, V. Valtchev, T. Bein, *Science* **1999**, *283*, 958.
[39] S. Mintova, N. Olson, T. Bein, *Angew. Chem.* **1999**, *111*, 3405; *Angew. Chem. Int. Ed.* **1999**, *38*, 3201.
[40] J. Yao, D. Li, X. Zhang, C. H. Kong, W. Yue, W. Zhou, H. Wang, *Angew. Chem.* **2008**, *120*, 8525; *Angew. Chem. Int. Ed.* **2008**, *47*, 8397.

Received: April 23, 2010
Published online: September 30, 2010

  